Solution Structure of the CIDE-N Domain of CIDE-B and a Model for CIDE-N/CIDE-N Interactions in the DNA Fragmentation Pathway of Apoptosis

Alexey A. Lugovskoy,*†‖ Pei Zhou,†‖ James J. Chou,†
John S. McCarty,‡ Peng Li,‡ and Gerhard Wagner†§
*Committee on Higher Degrees in Biophysics
Harvard University
Cambridge, Massachusetts 02138
†Department of Biological Chemistry
  and Molecular Pharmacology
Harvard Medical School
Boston, Massachusetts 02115
‡Laboratory for Apoptosis Regulation
Institute of Molecular and Cell Biology
30 Medical Drive
Singapore 117609
Singapore

Summary

Apoptotic DNA fragmentation and chromatin condensation are mediated by the caspase-activated DFF40/CAD nuclease, which is chaperoned and inhibited by DFF45/ICAD. CIDE proteins share a homologous regulatory CIDE-N domain with DFF40/CAD and DFF45/ICAD. Here we report the solution structure of CIDE-N of human CIDE-B. We show that the CIDE-N of CIDE-B interacts with CIDE-N domains of both DFF40 and DFF45. The binding epitopes are similar and map to a highly charged bipolar surface region of CIDE-B. Furthermore, we demonstrate that the CIDE-N of CIDE-B regulates enzymatic activity of the DFF40/DFF45 complex in vitro. Based on these results and mutagenesis data, we propose a model for the CIDE-N/CIDE-N complex and discuss the role of this novel bipolar interaction in mediating downstream events of apoptosis.

Introduction

Apoptosis, a morphologically distinct form of programmed cell death, is an evolutionary highly conserved phenomenon that plays an important role in the regulation of cellular activities in eukaryotes (Wylie et al., 1980). Various stimuli, such as cytokines and anticancer drugs, as well as growth factor deprivation and radiation damage, cause a cell to undergo a rapid, inflammatory-free clearance that is characterized by cell shrinkage, blebbing of plasma membranes, nuclear condensation, and DNA fragmentation (Earnshaw, 1995; Nagata, 1997; Green and Reed, 1998). Apoptosis consists of two stages: the stage of the commitment, when the target cell is being sentenced to death; and the stage of execution, when proteins, DNA, and other structural components of the cell are destroyed. Death signals originating from the death receptors, such as TNF and Fas, or mitochondria trigger the activation of Caspase 8 or Caspase
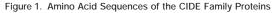
9, respectively. These activated initiator caspases, in turn, actuate the downstream executioner Caspases 3, 6, and 7 (Zou et al., 1997; Green, 1998). The cross-talk between the two pathways is mediated by BID, which upon cleavage by Caspase 8, can activate the mitochondrial pathway of cell death (Li et al., 1998; Luo et al., 1998).

DNA degradation and nuclear condensation are characteristic downstream events of apoptosis. They are triggered by a heterodimeric protein composed of a 40 kDa caspase-activated DNA fragmentation factor (DFF40/CAD) and its 45 kDa inhibitor (DFF45/ICAD) (Liu et al., 1997; Enari et al., 1998). Cleavage of DFF45/ICAD by Caspase 3 at two different sites releases DFF40/CAD from the complex and triggers DNA fragmentation and nuclear condensation (Liu et al., 1998; Sakahira et al., 1998). DFF40/CAD consists of two domains with distinct functions. Its C-terminal part exhibits DNA nuclease activity, whereas the N-terminal CIDE-N domain has a regulatory function (Inohara et al., 1999). Similarly, DFF45/ICAD contains an N-terminal CIDE-N domain (Figure 1A) that is sufficient to inhibit DNA fragmentation (Inohara et al., 1998). Additionally, CIDE-N of DFF45 exhibits chaperone activity on DFF40 by directly interacting with CIDE-N of DFF40 (McCarty et al., 1999a, 1999b), albeit other domains of DFF45 are required for its effective chaperone function (Gu et al., 1999; Sakahira et al., 1999).

Recently, a novel family of cell death–inducing DFF45-like effector (CIDE) proteins has been identified (Inohara et al., 1998). CIDEs share an N-terminal domain that is homologous to the CIDE-Ns of DFF40/CAD and DFF45/ICAD (Figure 1A). It has been shown that overexpression of CIDEs results in apoptosis (Inohara et al., 1998). Unlike DFF45 and DFF40, CIDE proteins are expressed in a highly restricted manner and show pronounced tissue specificity (Inohara et al., 1998). Besides the N-terminal domain (CIDE-N), CIDEs also contain a C-terminal killer domain (CIDE-C) (Figure 1B). Interestingly, while the proapoptotic function of full-length CIDEs is inhibited by DFF45, CIDE-C domains can induce apoptosis even in the presence of DFF45. Thus, it has been postulated that CIDE-N domains play a regulatory role in mediating CIDE-induced apoptosis by associating with other CIDE-N domain-containing proteins. However, no direct evidence for that interaction has been reported (Inohara et al., 1998).

The high degree of homology among the N-terminal regions of DFF40, DFF45, and CIDEs (Figure 1A) suggests a common regulatory role of CIDE-N domains in the DNA fragmentation pathway of apoptosis. To understand the molecular basis for CIDE-N function, we determined the solution structure of CIDE-N of human CIDE-B (Figures 2A and 2B). The structure consists of a twisted five-stranded β sheet and two α helices arranged in an α/β roll fold. Using NMR titration experiments, we showed that the CIDE-N of CIDE-B interacts with the CIDE-N domains of DFF45 and DFF40. Based on the chemical shift perturbation data, we mapped the binding surface of CIDE-N (CIDE-B) to the solvent-exposed face of the β sheet and a conserved EDG loop located on

§To whom correspondence should be addressed (e-mail: gerhard_wagner@hms.harvard.edu).
‖These authors contributed equally to this work.

A

B

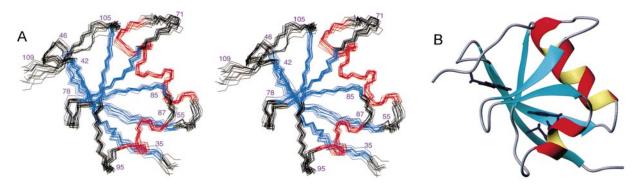Figure 1. Amino Acid Sequences of the CIDE Family Proteins

(A) Sequence alignment of different CIDE-N domains. The conserved and homologous residues are shown in black and gray, respectively. The secondary structure of the CIDE-N of CIDE-B is presented on the top; cylinders and arrows represent α helices and β strands, respectively. The residues of the CIDE-N domain of CIDE-B, which are perturbed upon binding to the CIDE-N domain of DFF45, are illustrated with asterisks.
(B) Functional domains of CIDE-B protein. CIDE-N and CIDE-C domains are shown in gray and black, respectively.
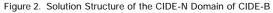
the same side of the molecule. This binding surface is highly polar and consists of two oppositely charged regions. The unusual juxtaposition of the large basic and acidic surfaces suggests a bipolar electrostatic mode for the CIDE-N/CIDE-N homophilic interaction. Additionally, CIDE-N (CIDE-B) can regulate the enzymatic activity of the DFF40/DFF45 complex, as shown by an in vitro DNA degradation assay. This further supports the significance of the CIDE-N homophilic interaction. Finally, based on the structure of CIDE-N domains, together with the chemical shift perturbation and mutagenesis data, we propose a novel mechanism for the CIDE-N/CIDE-N homophilic association, which involves complementary neutralization of two bipolar surfaces.

Results and Discussion

Structure Determination

Sequential resonance assignments of the CIDE-N domain of CIDE-B (residues 1–116) were achieved using

three pairs of triple resonance experiments [HNCA, HN(CO)CA, HNCO, HN(CA)CO, HN(CA)CB, HN(COCA) CB], ^{15}N selective labeling of valine, leucine, and isoleucine, and reverse labeling of arginine residues as described before (Chou et al., 1998). The structure of the CIDE-N of CIDE-B was determined using a total of 1206 distance constraints derived from 2D homonuclear NOESY and 3D ^{15}N or ^{13}C dispersed NOESY experiments and 210 angle constraints derived from the analysis of local NOE patterns and $^{3}J_{N\alpha}$ scalar coupling constants, measured in an HMQC-J experiment. Residues 1–31 and 111–122 were found to be unstructured based on transverse ^{15}N relaxation rates (data not shown) and the absence of long-range NOEs in these regions. Structures were calculated with a combined use of torsion angle dynamics (Güntert et al., 1997) and simulated annealing (Brünger, 1994). The quality of the determined structures can be assessed from the structural statistics of the ensemble of 15 calculated structures (Table 1 and Figure 2A).

Figure 2. Solution Structure of the CIDE-N Domain of CIDE-B

(A) Stereo view of the backbone atoms (N, C$^{\alpha}$, C^{O}) of the 15 superimposed NMR-derived structures of CIDE-N (CIDE-B) (residues 34–109). β strands and α helices are shown in blue and red, respectively.
(B) The ribbon diagram of CIDE-N (CIDE-B) (residues 34–109).

Table 1. Structural Statistics for the CIDE-N of CIDE-B

NOE distance restraints	
All	1120
Intraresidue	755
Sequential ($|i - j| = 1$)	194
Medium range ($|i - j| \leq 4$)	45
i, i + 2	11
i, i + 3	24
i, i + 4	10
Long range ($|i - j| \geq 5$)	116
H bond constraints[a]	96
Dihedral angle constraints[b]	210
Ramachandran plot[c]	
Most favorable region	83.4%
Additionally allows region	16.6%
Generously allowed region	0.0%
Disallowed region	0.0%
Average ensemble rmsd[d]	
Backbone (residues 35–108)	0.73 Å
Heavy atoms (residues 35–108)	1.29 Å

[a] Hydrogen bonds were added only at the late stage of structural calculations for residues with characteristic NOE patterns.
[b] Dihedral angle constraints were generated using DYANA (Güntert et al., 1997) based on $^3J_{\alpha N}$ couplings and NOE constraints.
[c] PROCHECK_NMR (Laskowski et al. 1996) was used to assess the quality of the structures.
[d] None of these structures exhibit distance violations greater than 0.2 Å or dihedral angle violations greater than 5°.

Structure Overview

The three-dimensional structure of the CIDE-N of CIDE-B is shown in Figure 2B. Regions 1–31 and 111–122 are omitted because they are largely disordered. The structured portion of the CIDE-N domain of CIDE-B has the fold of an α/β roll and consists of five β strands arranged in a single sheet and two α helices (Figure 1A). Strand 1 (residues 35–42) and strand 2 (residues 47–54) are connected by a short constrained loop (residues 43–46) and form a β hairpin. Helix 1 (residues 58–68) is packed against strands 3 (residues 74–77), 4 (residues 82–85), and 5 (residues 99–102), which are arranged in an anti-parallel orientation. Strand 5 and a portion of strand 1 (residues 39–42) pair in a parallel orientation and complete the assembly of the mixed β sheet. The structure is additionally stabilized by the packing of aromatic residues in the core of the domain. Phenylalanines 38, 89, and 90 are integrated into the hydrophobic core of the molecule, whereas tryptophane 108 constrains the C-terminal loop (residues 103–108) by contacting valine 76, alanine 83, and methionine 100 of strands 3 and 5. Aromatic residues in positions 90 and 108 are absolutely conserved within the CIDE family, and corresponding mutations in DFF40 resulted in the diminished nuclease activity of the enzyme (Inohara et al., 1999).

A search using the DALI server (Holm and Sander, 1993) revealed a similarity of the CIDE-N domain of CIDE-B to the Ras-binding domain (RBD) of Raf-1 kinase (Protein Data Bank ID code 1c1y-B) with a Z score of 2.7, although no sequence similarity exists between the proteins. Both molecules have an α/β roll type of fold with an average rms deviation of 3.4 Å between superimposed backbone atoms. The RBD fold has also been classified as a ubiquitin fold (Nassar et al., 1995); however, the DALI search did not identify ubiquitin as a fold related to the CIDE-N domain of CIDE-B.

The CIDE-N Domain of CIDE-B Binds DFF40 and DFF45 CIDE-N Domains

Previously, association between CIDE-N domains of DFF40 and DFF45 has been observed (McCarty et al., 1999a, 1999b), and interaction between CIDE-N of CIDE-A and DFF45 has been postulated (Inohara et al., 1998). Thus, we explored the possibility of the interaction between CIDE-N (CIDE-B) and the homologous domains of DFF40 and DFF45. We performed titration experiments by recording ^1H-^{15}N HSQC spectra of ^{15}N-labeled CIDE-N (CIDE-B) in the presence of an excess of unlabeled CIDE-N domains of DFF40 and DFF45. Interestingly, we found that CIDE-Ns of both DFF40 and DFF45 bind to the same face of the CIDE-N domain of CIDE-B. Resonances of residues 39–55, 78–81, 87, 91, 96–97, 99–101, and 105 were perturbed upon binding of either CIDE-N (DFF40) or CIDE-N (DFF45) (Figure 3D). In addition, residue 36 was affected in the titration with CIDE-N (DFF45), but not with CIDE-N (DFF40), indicating a slight difference in the location and size of the binding face. The analysis of the perturbation patterns revealed that residues in strands 1 and 2 (residues 36, 39–55) and the conserved loop residues 78–81 and 96–97 are affected most, and thus they constitute the bulk of the interaction interface. Residues 87, 91, and 105 are adjacent but peripheral to the main binding face. It is possible that these residues located in the loop regions experience long-range effects. Perturbations in strand 5 (residues 99–102) may represent a secondary effect, as strand 5 pairs with strand 1, which is involved in the interaction. The perturbation pattern suggests that some local rearrangements occur upon binding; however, the overall structural integrity is preserved, as the only residues affected outside of strands 1, 2, and 5 are located in loop regions, and the resonances of the residues involved in the hydrophobic core formation remain unchanged.

The analysis of the interaction surface of CIDE-N (CIDE-B) with CIDE-N domains of DFF40 and DFF45 (Figures 3A and 3B) shows that the perturbed residues are localized on one side of the molecule and are clustered into two regions. The bottom region in the orientation of Figure 3A encompasses strands 1 and 2 (residues 36, 39–53), and the top region includes residues 78–81 and 96–97. Interestingly, these two regions coincide with two areas of opposite charge in an electrostatic surface plot (Figure 4A), suggesting a possibility of an electrostatic mode for the CIDE-N/CIDE-N interaction.

CIDE-N (CIDE-B) Can Regulate the Enzymatic Activity of the DFF40/DFF45 Complex

DFF45 efficiently inhibits DFF40 nuclease activity through the collective high-affinity binding of its multiple domains to DFF40 (McCarty et al., 1999a, 1999b). Inhibition, however, can be achieved by the independent binding of the CIDE-N domain of DFF45 to the regulatory domain of DFF40 at stoichiometric excess (McCarty et al., 1999a, 1999b). We used an in vitro plasmid degradation assay to investigate the effect of CIDE-N (CIDE-B) domain on the interaction of DFF40/DFF45 CIDE-N domains. In this assay, full-length DFF40 was incubated with plasmid DNA in the presence of different amounts of CIDE-N (DFF45) and CIDE-N (CIDE-B), and the cleavage products were analyzed by gel electrophoresis on
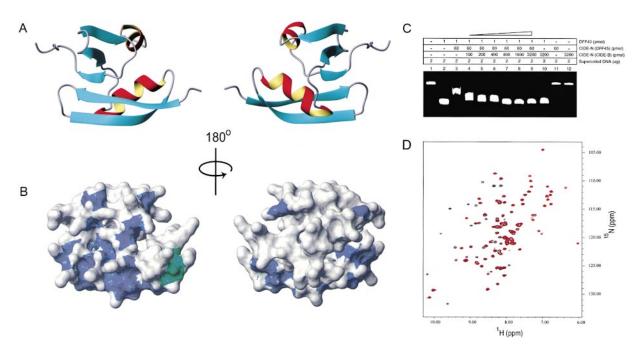
Figure 3. CIDE-N (CIDE-B) Interacts with CIDE-N Domains of Both DFF40 and DFF45

(A) Ribbon diagram of CIDE-N (CIDE-B) is presented in two views different by 180° rotation around the y axis.

(B) Surface plot of CIDE-N (CIDE-B). The amides involved in the interaction with both DFF40 and DFF45 are colored in blue; amide of residue 36 additionally involved in binding of DFF45 is colored in green. Orientation and views are the same as in (A).

(C) In vitro plasmid degradation assay. CIDE-N (CIDE-B) does not significantly affect the nuclease activity of DFF40, but it reverses the inhibition of DFF40 by the CIDE-N domain of DFF45. DFF40 cleaves supercoiled plasmid (lane 1) into ca. 80 bp fragments (lane 2). This activity is strongly inhibited by the CIDE-N domain of DFF45 (lane 3). Increasing concentrations of the CIDE-N of CIDE-B (lanes 4–9) reverse the inhibition of DFF40 by the CIDE-N domain of DFF45. High concentrations of the CIDE-N domain of CIDE-B, however, did not significantly inhibit DFF40 nuclease activity (lane 10). CIDE-N domains of neither DFF45 nor CIDE-B exhibit activity under these conditions (lanes 11 and 12).

(D) Overlay of ^{1}H-^{15}N HSQC spectra of ^{15}N-labeled CIDE-N (CIDE-B) in absence (shown in black) and presence (shown in red) of the excess of the unlabeled CIDE-N domain of DFF45.

2% agarose gels (Figure 3C). In contrast to the strong inhibition observed for the CIDE-N domain of DFF45, the CIDE-N of CIDE-B had little effect. However, it was able to rescue the enzymatic activity of DFF40 previously inhibited by CIDE-N (DFF45). Combined with the results of NMR binding studies, this indicates that CIDE-N (CIDE-B) is capable of sequestering CIDE-N (DFF45) from the regulatory domain of DFF40, thus restoring the nuclease function. The opposite effects of CIDE-N domains of DFF45 and CIDE-B on DFF40 enzymatic activity may originate from their distinct surface properties and different on/off rates in CIDE-N/CIDE-N complexes (discussed below). Our observations verify the interaction between CIDE-B and the DFF40/DFF45 complex and raise the possibility that multiple pathways exist in regulation of DNA fragmentation in apoptosis.

Modeling of DFF40 and DFF45 CIDE-N Domains and the CIDE-N/CIDE-N Interaction

To further elucidate the mechanism of the CIDE-N/CIDE-N interaction, we modeled the structures of CIDE-N domains of DFF40 and DFF45. Since the CIDE-N domains are 60% homologous (Figure 1A), it is possible to employ the segment matching method (Levitt, 1992) using the backbone of CIDE-N (CIDE-B) as a framework to model CIDE-N domains of DFF40 and DFF45. We followed the procedure described in Chou et al (1998). Twenty target structures of CIDE-N (DFF40) and of

CIDE-N (DFF45) were calculated using the program package Look (Levitt, 1995). The average structures were then subjected to energy minimization using the program ENCAD (Levitt, 1983) to ensure the correct stereochemistry and the absence of van der Waals distances violations. The resulting models of CIDE-N (DFF40) and CIDE-N (DFF45) were similar to CIDE-N (CIDE-B), and they exhibited a similar surface charge polarity on the face similar to the binding interface of the CIDE-N of CIDE-B (Figures 4B and 4C). Interestingly, in all three CIDE-Ns, the positively charged area has a convex shape, whereas the negatively charged part is concave, which further supports our hypothesis that CIDE-N domains interaction is electrostatically driven. The tight fit between oppositely charged surfaces of complementary shape would increase the interaction strength, since it will eliminate the water molecules from the interface.

To validate our modeling results, we obtained the backbone resonance assignments of CIDE-N (DFF40) and performed titrations experiments by recording ^{1}H-^{15}N HSQC spectra of ^{15}N-labeled CIDE-N (DFF40) in the presence of various concentrations of unlabeled CIDE-N domains of DFF45 and CIDE-B (data not shown). The established interaction interfaces of CIDE-N (DFF40) with both CIDE-N (DFF45) and CIDE-N (CIDE-B) encompass the bipolar region and are similar to the interaction interfaces obtained for CIDE-N (CIDE-B).
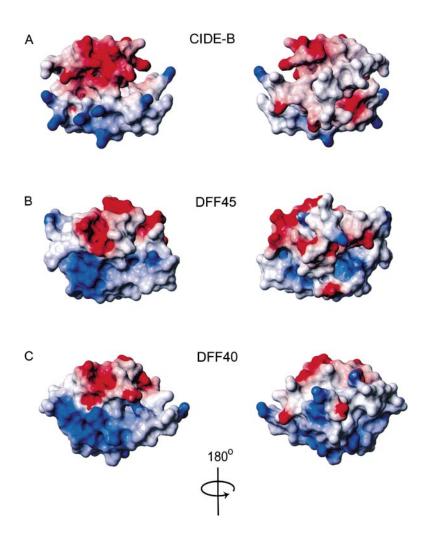
Figure 4. The Binding Face of CIDE-N Domain Possesses a Distinct Polarity with Two Clusters of Opposite Charge Located on the Same Side of the Molecule

(A) Electrostatic potential map of CIDE-N (CIDE-B). Regions of negative and positive charge are shown in red and blue, respectively. Orientation and views are similar to Figure 3A.

(B) Electrostatic potential map of CIDE-N (DFF45). Regions of negative and positive charge are shown in red and blue, respectively. Orientation and views are similar to Figure 3A.

(C) Electrostatic potential map of CIDE-N (DFF40). Regions of negative and positive charge are shown in red and blue, respectively. Orientation and views are similar to Figure 3A.

Using the knowledge of the electrostatic properties of CIDE-N domains and the maps of the interaction surfaces, we constructed a model of CIDE-N (DFF45) in complex with CIDE-N (CIDE-B). In our procedure, we aligned the molecules in a way that involves complementary neutralization of two bipolar surfaces and maximizes their surface complementarity. The resulting model of the CIDE-N/CIDE-N complex obtained in this way is presented on Figure 5. CIDE-N domains of CIDE-B and DFF45 are arranged in a yin/yang-like configuration so that the acidic (EDG loop) and basic (strands 1 and 2) surfaces of the opposite domains contact each other. The bipolar mode of the electrostatic interaction is compatible with the surface properties of the molecules as the convex positively charged area is accommodated into the negatively charged pocket. The electrostatic nature of the interaction is consistent with a relatively low affinity (K_D in μM range) and relatively fast on/off rates of the CIDE-N/CIDE-N interaction (McCarty et al., 1999a, 1999b). This is similar to the characteristics found for other interactions dominated by electrostatic component, such as the CD2/CD58 interaction (Sun et al., 1999; Wang et al., 1999) or the CARD/CARD interaction (Chou et al., 1998; Qin et al., 1999; Zhou et al., 1999). Based on the high degree of sequence homology within CIDE family and preserved surface polarity, we propose that other CIDE-N domains (e.g., CIDE-N domains of DFF45 and DFF40) will interact in a similar fashion (Figure 5).

Specificity of the CIDE-N/CIDE-N Interactions
Multiple lines of biochemical evidence suggest that CIDE-N domains from different proteins interact with each other. CIDE-Ns of DFF40 and DFF45 were shown to interact (Inohara et al., 1999; McCarty et al., 1999a, 1999b). In our study, we have demonstrated the binding of the CIDE-N of CIDE-B to the CIDE-N domains of DFF45 and DFF40. Additionally, an interaction between CIDE-A and CIDE-B has been observed (P. L., unpublished data). We have demonstrated that two clusters of oppositely charged residues located on the same side of the protein are involved in the formation of the CIDE-N/CIDE-N complex. Given our modeling results and conservation of the positively and negatively charged residue patterns within the CIDE-N family, we suggest that the CIDE-N/CIDE-N interaction is driven by electrostatic forces. However, affinities vary for different CIDE-N/CIDE-N complexes, such as DFF40/DFF45, DFF45/CIDE-B, and DFF40/CIDE-B (P. L., unpublished data). Comparison between CIDE-N domains of DFF40, DFF45, and CIDE-B revealed their various surface properties. We suggest that different degrees of surface and charge complementarity can modulate the propensities for association, thus providing the fine-tuning of the
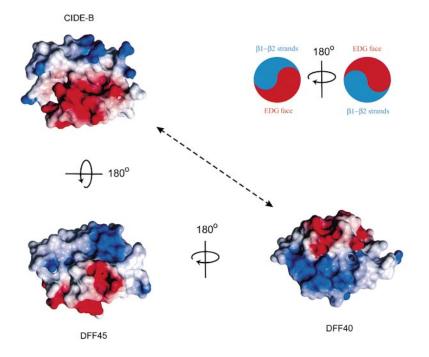
CIDE-B

DFF45

DFF40

Figure 5. A Model for the CIDE-N/CIDE-N Homophilic Interaction

CIDE-N domains associate in a yin/yang-like orientation with the EDG face of one molecule packing against strands 1 and 2 of the other one. Regions of positive and negative charge are shown in blue and red, respectively. The 180° rotation operations to form the putative complexes are indicated with arrows. The dashed line represents a weaker interaction between CIDE-N domains of CIDE-B and DFF40.

bipolar interaction in CIDE-N/CIDE-N complexes. This notion may explain different effects of CIDE-N domains of DFF45 and CIDE-B on the function of DFF40. The CIDE-N/CIDE-N interaction between DFF40 and CIDE-B is weaker than those between DFF45 and CIDE-B or DFF40 and DFF45. Thus, even in the presence of CIDE-N (CIDE-B), the regulatory and catalytic domains of DFF40 can associate and trigger the nuclease activity, whereas CIDE-N (DFF45) would inhibit the enzyme.

On the functional level, the binding specificity of CIDE family proteins may come from synergistic interactions between multiple protein domains. It has been reported that the C-terminal domain of DFF45 binds the catalytic domain of DFF40 (Gu et al., 1999; McCarty et al., 1999a, 1999b; Sakahira et al., 1999). On the other hand, CIDE-N domains were shown to be essential for enzymatic activity of DFF40, chaperone activity of DFF45, and regulation

of CIDE-induced apoptosis (Inohara et al., 1998, 1999; McCarty et al., 1999a, 1999b). This data combined with an observation of fast on/off rates for CIDE-N/CIDE-N interactions (McCarty et al., 1999a, 1999b) suggest that CIDE-Ns can generally act as "bait" domains providing initial low-affinity recognition, whereas tight and specific binding originates from a slow association of multiple "anchor" domains.

Comparison of CIDE-N/CIDE-N Interaction to Other Homophilic Interaction in Apoptosis

So far, three classes of homophilic interactions relevant for regulation of apoptosis have been described (Hofmann et al., 1997). The death domain (DD), death effector domain (DED), and caspase recruitment domain (CARD) are involved in the regulation of early events in apoptosis (reviewed by Liang and Fesik, 1997; Nagata, 1997). Three-dimensional structures of several of these domains have been determined (Huang et al., 1996; Chou et al., 1998; Eberstadt et al., 1998). DD, DED, and CARD are composed of six closely packed antiparallel α helices, and their surfaces have distinct electrostatic polarities. DD/DD, DED/DED, and CARD/CARD interactions are very selective, as any particular domain interacts only with its partner, but not with other members of the family. Electrostatic interactions have been implicated to provide both driving force and specificity filters for DED/DED and CARD/CARD interactions. Similarly CIDE-N/CIDE-N interactions have electrostatic character, but their specificity is limited, which can be representative of their deployment in the execution process rather than in initiation stage of apoptosis. Another difference between these homophilic interaction domains is the surface charge distribution: DED and CARD have two oppositely charged surfaces, whereas both positive and negative charge clusters of CIDE-N are located on the same side of the molecule, making another face available for additional function. These observations suggest

WT-DFF40   E50A-DFF40   D51A-DFF40

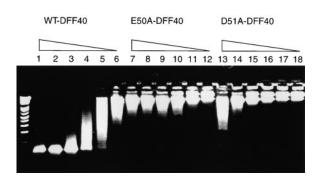1 2 3 4 5 6   7 8 9 10 11 12   13 14 15 16 17 18

Figure 6. Point Mutations E50A and D51A Lead to the Diminished Enzymatic Activity of DFF40 in a Cell-Free System

Constant concentrations of plasmid DNA (0.1 μg/μl) are treated with a series of 2-fold dilutions of WT-DFF40 (lane 1–6), E50A-DFF40 (lane 7–12), and D51A-DFF40 (lane 13–18), respectively, in the absence of DFF45. The concentrations of the enzyme were carefully normalized by Western blotting. The experiment was performed similarly to the plasmid degradation assay (described in Experimental Procedures).
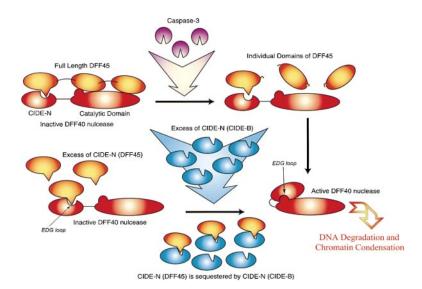
Figure 7. A Model for the Inhibition and Activation of DFF40 Nuclease

Caspase 3 cleaves DFF45 into three domains that dissociate from the DFF40/DFF45 complex (top). Subsequently, the EDG loop of the CIDE-N domain of DFF40 interacts with the catalytic domain of nuclease, triggering DNA degradation and chromatin condensation. DFF40 can be inhibited by an excess of CIDE-N (DFF45). However, excess CIDE-N (CIDE-B) can sequester the CIDE-N domain of DFF45, making the EDG loop of DFF40 available for the interaction with nuclease catalytic domain (bottom).

that the CIDE-N/CIDE-N interaction is a novel type of homophilic interaction involved in the regulation of apoptosis.

Multiple Roles of the CIDE-N Domain in DFF40 Nuclease

The structural information allowed us to rationalize the mutagenesis data available for the conserved residues of the CIDE-N domain of DFF40. Substitutions K32A, L48P, and T53L have no effect on the enzymatic function, whereas mutations E50A, D51A, G52I, F60S, and W78C (in the numbering of human DFF40 as in Figure 1A) result in the diminished nuclease activity (Inohara et al., 1999; P. L., unpublished data). Lysine 32 (located in the helix 1) is remote to the interaction interface and has no obvious function. Leucine 48 and threonine 53 are terminal residues of strands 3 and 4. The hydrophobic contacts of their side chains are important for the constraining of the conserved EDG loop. Thus, mutations preserving the hydrophobicity of these residues may not affect the nuclease activity.

The conserved aromatic residues phenylalanine 60 and tryptophane 78 are involved in the formation of the hydrophobic core of the molecule; therefore, mutations in these positions can reduce the enzyme stability. Glycine 52 adopts a conformation with positive ϕ angle, which is not readily accessible for isoleucine. Thus, the G52I mutation may alter the conformation of the negatively charged EDG loop, which is important for CIDE-N/CIDE-N interactions.

An interesting observation comes from the analysis of the E50A and D51A mutants. Glutamate 50 and aspartate 51 are located on the top of the hairpin between strands 3 and 4 and are essential for the CIDE-N/CIDE-N interactions. Thus, these mutations should lead to the activation of DFF40, as they are expected to disrupt the DFF40/DFF45 complex. Nevertheless, both E50A and D51A mutants exhibit reduced catalytic potency. To address the mode of DFF40 activation, we have compared the nuclease activity of these two mutants in a cell-free system (Figure 6) with the wild-type enzyme in the absence of DFF45. The levels of the enzyme have been carefully normalized by Western blotting. Both mutants

show the diminished nuclease activity, which cannot be attributed to any additional factors interacting with DFF40. Therefore, it results from the disrupted self-assembly of DFF40. The backbone resonance assignment of the CIDE-N (DFF40) reveals that E50 and D51 are located in the loop region, so it is unlikely that the mutagenesis altered the structure and the stability of the protein. It has been hypothesized (Inohara et al., 1999) that the CIDE-N domain of DFF40 can act as an activator domain for the nuclease. Our results indicate that residues of the conserved EDG loop are important for the enzymatic activity, possibly by being involved in direct interaction between regulatory and catalytic domains of DFF40.

The model for DFF40 activation is shown in Figure 7. Full-length DFF45 inhibits DFF40 by the synergistic binding of its three domains to both activator and catalytic domains of the nuclease. Caspase 3 cleaves DFF45 into three individual domains, which dissociate away from DFF40. The N-terminal domain of DFF45 binds the activator domain of DFF40 and is sufficient for the inhibition; however, due to the competition with the catalytic domain of the nuclease, an excess of CIDE-N (DFF45) is required. The CIDE-N domain of CIDE-B can sequester CIDE-N (DFF45) and thus is able to rescue the nuclease activity. The observation that the mutations in the EDG loop reduce nuclease activity in the absence of DFF45 suggests that the EDG loop of CIDE-N (DFF40) interacts with the catalytic domain of the nuclease (Figure 7).

Thus, the CIDE-N domain of DFF40 has multiple functions. In the absence of apoptotic stimuli, it is recognized by DFF45 for chaperoning and inhibition purposes. On the other hand, once the death signal is received and DFF45 is proteolysed by Caspase 3, it functions as an activator domain interacting with the catalytic domain of DFF40 and triggering DNA degradation and chromatin condensation.

Conclusion

CIDE-N domains are involved in the regulation of downstream events in apoptosis. Their homophilic interactions have been shown to mediate proapoptotic activity

of CIDE proteins, nuclease activity of DFF40, and inhibitory and chaperone activity of DFF45 (Inohara et al., 1998, 1999; McCarty et al., 1999a, 1999b). We have determined the three-dimensional structure of the CIDE-N domain of the human CIDE-B protein. The structure consists of a five-stranded twisted β sheet and two α helices with a topology of an α/β roll. The interaction interfaces of the CIDE-N domain of CIDE-B with CIDE-N domains of DFF40 and DFF45 have been found to be similar. They have been mapped to the solvent-exposed face of strands 1 and 2 and the conserved EDG loop residues located on the same side of the CIDE-N domain of CIDE-B. This binding face is highly charged and consists of two clusters of the opposite polarity. Homology modeling of DFF40 and DFF45 using a segment matching method (Levitt, 1992) has shown that this surface polarity is conserved among the CIDE-N domains. Based on NMR titration data and electrostatic potential maps, we present a general model for a CIDE-N/CIDE-N complex. CIDE-N domains associate in a yin/yang-like orientation, which involves neutralization of two bipolar surfaces and maximizes their surface complementarity. Finally, having compared CIDE-N/CIDE-N interaction with other homophilic interactions involved in the regulation of apoptosis, we conclude that CIDE-N/CIDE-N represents a novel type of homophilic interaction which mediates downstream events of apoptosis.

Experimental Procedures

Overexpression and Purification of CIDE-N (CIDE-B) (1–116), CIDE-N (DFF40) (1–80), and CIDE-N (DFF45) (1–116)

The CIDE-N of human CIDE-B (1–116) (GenBank accession number AF190901) was subcloned into pET-15b vector using NcoI/NdeI restriction sites. CIDE-N (CIDE-B) was expressed in *Escherichia coli* as C-terminal His-tag fusion protein. The transformed cells were grown at 37°C and induced with 1 mM IPTG in either LB media (for unlabeled protein) or M9-minimal media substituted with ^{15}N-NH$_4$Cl (1 g/l) for ^{15}N-labeled protein and ^{13}C-glucose (2 g/l) for uniform ^{13}C labeling. A 90% deuterated, uniformly ^{15}N, ^{13}C labeled protein was prepared by growing the cells in 90% D$_2$O supplemented with ^{15}N-NH$_4$Cl and ^{13}C-glucose. Selective labeling of valine, leucine, and isoleucine was obtained by growing cells in M9 media with 100 mg/l ^{15}N-labeled corresponding amino acid. Reverse labeling of arginine was obtained by growing cells in M9 media substituted with ^{15}N-NH$_4$Cl (1 g/l) and addition of 100 mg/l of unlabeled arginine. 10% ^{13}C labeled sample was obtained using M9 media (containing 2 g/l glucose) supplemented with 0.2 g/l ^{13}C-glucose.

After cell lysis, the histidine tag-fused recombinant protein was purified using Ni^{2+}-NTA affinity chromatography according to standard protocol. The eluted CIDE-N (CIDE-B) was further purified to homogeneity using gel filtration (Sephadex G-75) and then exchanged into NMR buffer containing 50 mM phosphate (pH 6.6) in H$_2$O/D$_2$O (9/1) or D$_2$O.

CIDE-N (DFF40) (1–80) and CIDE-N (DFF45) (1–116) were subcloned into pET-15b vector as C-terminal and N-terminal His-tag fusion proteins, respectively. Both proteins were expressed and purified as described above. The backbone resonance assignment of CIDE-N (DFF40) was obtained as described above.

NMR Spectroscopy

All NMR spectra were acquired at 25°C on Bruker DRX 500, Bruker DRX 600, Varian Unity 500, or Varian Inova 750 spectrometers. Sequential assignments were achieved using three pairs of triple-resonance experiments, [HNCA, HN(CO)CA], [HNCO, HN(CA)CO], and [HN(CA)CB, HN(COCA)CB] using uniformly ^{15}N, ^{13}C-labeled and 90% deuterated protein in 90%H$_2$O/10% D$_2$O (for reviews, see Clore and Groneborn, 1994; Yamazaki et al., 1994). In addition, amino acid–selective ^{15}N labeling of valine, isoleucine, and leucine and reverse

labeling of arginine were used to confirm the sequential assignment of amide protons. Side chain proton resonances were mostly assigned using 3D Cbd-HCCH-TOCSY (Matsuo et al., 1997) and 3D ^{15}N-dispersed TOCSY-HSQC spectra, recorded using uniformly ^{13}C-labeled protein in D$_2$O and uniformly ^{15}N-labeled protein in H$_2$O, respectively. The assignment of aromatic side chains was accomplished using homonuclear TOCSY and NOESY experiments, acquired on the nonlabeled protein in D$_2$O. Stereo-specific assignment of methyl groups of valine, isoleucine, and leucine was obtained from ^{13}C-HSQC spectrum of a 10% ^{13}C-labeled protein (Szypserski et al., 1992). ^{3}J$_{\alpha N}$ couplings were obtained through an HMQC-J experiment (Bax et al., 1983).

NMR Binding Studies of CIDE-N/CIDE-N Interaction

CIDE-Ns of CIDE-B, DFF40, and DFF45 were exchanged into NMR buffer before titration. A series of ^{1}H-^{15}N HSQC spectra were recorded by adding different amounts of nonlabeled CIDE-Ns of DFF40 and DFF45 into 100 μM ^{15}N-labeled CIDE-N of CIDE-B. NMR samples were equilibrated at room temperature for at least 1 hr before recording the NMR spectra.

Structural Calculation

Interproton distance constraints were derived from NOESY cross-peak volumes, which were autocalibrated using the CALIBA module included in the DYANA package (Güntert et al., 1997). Dihedral angle constraints were generated using HABAS based on ^{3}J$_{\alpha N}$ couplings and NOE patterns. Initial structures were generated using the program DYANA starting from random conformations and refined using simulated annealing protocol in X-PLOR. Loose hydrogen bond constraints were introduced at the late state of structural calculation and based on the characteristic NOE patterns observed for α helix β strand conformations. Of the 30 calculated structures, the 15 best with no NOE violation >0.2 Å and no dihedral angle violations >5.0° were presented in Figure 2 and were used to generate the statistics (Table 1). Figures were generated using MOLMOL program (Koradi et al., 1996).

DFF40 Enzymatic Assay and Inhibition Assay

Plasmid DNase assay was performed in 20 μl reactions containing 2 μg supercoiled maxiprep DNA in buffer A (100 mM KCl, 5 mM MgCl$_2$, and 1 mg/ml BSA). DFF40 was diluted in buffer A containing 50% glycerol and was added in 2.5 μl to the reaction (glycerol was not found to substantially effect the DNase reaction at concentrations up to 20%). CIDE-N (DFF45) and CIDE-N (CIDE-B) were diluted in buffer A and added in 5 μl. DFF40 (1 pmol) and effector proteins were preincubated 15 min at 37°C prior to the addition of DNA. After 30 min incubation at 37°C, DNA loading dye containing 50 mM EDTA was added and the DNA fragments separated on a 2% agarose gel by electrophoresis for 10 min at 150 V.

References

Bax, A., Griffey, R.H., and Hawkins, B.L. (1983). Correlation of proton and nitrogen-15 chemical shifts by multiple quantum NMR. J. Magn. Res. *55*, 301–315.

Brünger, A.T. (1994). XPLOR manual 3.851: a system for X-ray crystallography and NMR. X-PLOR Version 3.851 (New Haven, CT: Yale University Press).

Chou, J.J., Matsuo, H., Duan, H., and Wagner, G. (1998). Solution

structure of the RAIDD CARD and model for CARD/CARD interaction in caspase-2 and caspase-9 recruitment. Cell *94*, 171–180.

Clore, G.M., and Groneborn, A.M. (1994). Multidimensional heteronuclear nuclear magnetic resonance of proteins. Methods Enzymol. *239*, 349–363.

Earnshaw, W.C. (1995). Nuclear changes in apoptosis. Curr. Opin. Cell. Biol. *7*, 337–343.

Eberstadt, M., Huang, B., Chen, Z., Meadows, R.P., Ng, S.C., Zheng, L., Lenardo, M.J., and Fesik, S.W. (1998). NMR structure and mutagenesis of the FADD (Mort1) death-effector domain. Nature *392*, 941–945.

Enari, M., Sakahira, H., Yokoyama, H., Okawa, K., Iwamatsu, A., and Nagata, S. (1998). A caspase-activated DNase that degrades DNA during apoptosis, and its inhibitor ICAD. Nature *391*, 43–50.

Green, D.R. (1998). Apoptotic pathways: the roads to ruin. Cell *94*, 695–698.

Green, D.R., and Reed, J.C. (1998). Mitochondria and apoptosis. Science *281*, 1309–1312.

Gu, J., Dong, R.-P., Zhang, C., McLaughlin, D.F., Wu, M.X., and Schlossman, S.F. (1999). Functional interaction of DFF35 and DFF45 with caspase-activated DNA fragmentation nuclease DFF40. J. Biol. Chem. *274*, 20759–20762.

Güntert, P., Mumenthaler, C., and Wüthrich, K. (1997). Torsion angle dynamics for NMR structure calculation with the new program DYANA. J. Mol. Biol. *273*, 283–298.

Hofmann, K., Bucher, P., and Tschopp, J. (1997). The CARD domain: a new apoptotic signaling motif. Trends Biochem. Sci. *22*, 155–156.

Holm, L., and Sander, C. (1993). Protein structure comparison by alignment of distance matrices. J. Mol. Biol. *233*, 123–138.

Huang, B., Eberstadt, M., Olejniczak, E.T., Meadows, R.P., and Fesik, S.W. (1996). NMR structure and mutagenesis of the Fas (APO-1/CD95) death domain. Nature *384*, 638–641.

Inohara, N., Koseki, T., Chen, S., Wu, X., and Nunez, G. (1998). CIDE, a novel family of cell death activators with homology to the 45 kDa subunit of the DNA fragmentation factor. EMBO J. *17*, 2526–2533.

Inohara, N., Koseki, T., Chen, S., Benedict, M.A., and Nunez, G. (1999). Identification of regulatory and catalytic domains in the apoptosis nuclease DFF40/CAD. J. Biol. Chem. *274*, 270–274.

Koradi, R., Billeter, M., and Wüthrich, K. (1996). MOLMOL: a program for display and analysis of macromolecular structures. J. Mol. Graph. *14*, 51–55.

Laskowski, R.A., Rullmann, J.A., MacArthur, M.W., Kaptein, R., and Thorton, J.M.J. (1996). AQUA and PROCHECK_NMR: programs for checking the quality of protein structures solved by NMR. J. Biomol. NMR *8*, 477–486.

Levitt, M. (1983). Molecular dynamics of native protein: I. computer simulation of trajectories. J. Mol. Biol. *168*, 595–620.

Levitt, M. (1992). Accurate modeling of protein conformation by automatic segment matching. J. Mol. Biol. *226*, 507–523.

Levitt, M. (1995). Look, version 2.0. Molecular Application Group (Stanford University and Yeda).

Li, H., Zhu, H., Xu, C.J., and Yuan, J. (1998). Cleavage of BID by caspase 8 mediates the mitochondrial damage in the Fas pathway of apoptosis. Cell *94*, 491–501.

Liang, H., and Fesik, S.W. (1997). Three-dimensional structures of proteins involved in programmed cell death. J. Mol. Biol. *274*, 291–302.

Liu, X., Zou, H., Slaughter, C., and Wang, X. (1997). DFF, a heterodimeric protein that functions downstream of caspase-3 to trigger DNA fragmentation during apoptosis. Cell *89*, 175–184.

Liu, X., Li, P., Widlak, P., Zou, H., Luo, X., Garrard, W.T., and Wang, X. (1998). The 40-kDa subunit of DNA fragmentation factor induces DNA fragmentation and chromatin condensation during apoptosis. Proc. Natl. Acad. Sci. USA *95*, 8461–8466.

Luo, X., Budihardjo, I., Zou, H., Slaughter, C., and Wang, X. (1998). Bid, a Bcl2 interacting protein, mediates cytochrome c release from mitochondria in response to activation of cell surface death receptors. Cell *94*, 481–490.

Matsuo, H., Li, H., McGuire, A.B., Fletcher, C.M., Gingras, A., Sonenberg, N., and Wagner, G. (1997). Structure of translation factor eIF4E bound to m7GDP and interaction with the 4E-binding protein. Nat. Struct. Biol. *4*, 717–724.

McCarty, J.S., Toh, S.Y., and Li, P. (1999a). Study of DFF45 in its role of chaperone and inhibitor: two independent inhibitory domains of DFF40 nuclease activity. Biochem. Biophys. Res. Commun. *264*, 176–180.

McCarty, J.S., Toh, S.Y., and Li, P. (1999b). Multiple domains of DFF45 bind synergistically to DFF40: roles of caspase cleavage and sequestration of activator domain of DFF40. Biochem. Biophys. Res. Commun. *264*, 181–185.

Nagata, S. (1997). Apoptosis by death factor. Cell *88*, 355–365.

Nassar, N., Horn, G., Hermann, C., Scherer, A., McCormick, F., and Wittinghofer, A. (1995). The 2.2 Å crystal structure of the Ras-binding domain of the serine/threonine kinase c-Raf1 in complex with Rap1A and GTP analog. Nature *375*, 554–560.

Qin, H., Srinivasula, S.M., Wu, G., Fernandes-Alnemri, T., Alnemri, E.S., and Shi, Y. (1999). Structural basis of procaspase-9 recruitment by the apoptotic protease-activating factor 1. Nature *399*, 549–557.

Sakahira, H., Enari, M., and Nagata, S. (1998). Cleavage of CAD inhibitor in CAD activation and DNA degradation during apoptosis. Nature *391*, 96–99.

Sakahira, H., Enari, M., and Nagata, S. (1999). Functional differences of two forms of the inhibitor of caspase-activated DNase, ICAD-L, and ICAD-S. J. Biol. Chem. *274*, 15740–15744.

Sun, Z.-Y.J., Dötsch, V., Kim, M., Li, J., Reinherz, E.L., and Wagner, G. (1999). Functional glycan-free adhesion domain of human cell surface receptor CD58: design, production and NMR studies. EMBO J. *18*, 2941–2949.

Szypserski, T., Neri, D., Leiting, B., Otting, G., and Wuthrich, K. (1992). Support of ¹H NMR assignments in proteins by biosynthetically directed fractional ¹³C-labeling. J. Bio. NMR *2*, 323–334.

Wang, J.H., Smolyar, A., Tan, K., Liu, J.H., Kim, M., Sun, Z.Y., Wagner, G., and Reinherz, E.L. (1999). Structure of a heterophilic adhesion complex between the human CD2 and CD58 (LFA-3) counterreceptors. Cell *97*, 791–803.

Wylie, A.H., Kerr, J.F.R., and Currie, A.R. (1980). Cell death: the significance of apoptosis. Int. Rev. Cytol. *68*, 251–306.

Yamazaki, T., Lee, W., Arrowsmith, C.H., Muhandiram, D.R., and Kay, L.E. (1994). A suite of triple resonance NMR experiments for the backbone assignment of ¹⁵N, ¹³C, ²H labeled proteins with high sensitivity. J. Am. Chem. Soc. *116*, 11655–11666.

Zhou, P., Chou, J., Olea, R.S., Yuan, J., and Wagner, G. (1999). Solution structure of Apaf-1 CARD and its interaction with caspase-9 CARD: a structural basis for specific adaptor/caspase interaction. Proc. Natl. Acad. Sci. USA *96*, 11265–11270.

Zou, H., Henzel, W.J., Liu, X., Lutschg, A., and Wang, X. (1997). Apaf-1, a human protein homologous to C. elegans CED-4, participates in cytochrome c-dependent activation of caspase-3. Cell *90*, 405–413.

Protein Data Bank ID Code

The coordinates were deposited with the ID code 1d4b.